Original paper

Geology, mineralogy and possible origin of the copper mineralization in marble near Saldán, Córdoba (Argentina)

Fernando COLOMBO[1*], Raúl LIRA[2], Edward M. RIPLEY[3], José GONZÁLEZ DEL TÁNAGO[4]

[1] *CONICET, Cátedra de Geología General, Facultad de Ciencias Exactas, Físicas y Naturales – Universidad Nacional de Córdoba, Av. Vélez Sarsfield 1611 (X5016GCA) Córdoba, Argentina; fosfatos@yahoo.com.ar*

[2] *CONICET, Museo de Mineralogía. Facultad de Ciencias Exactas, Físicas y Naturales – Universidad Nacional de Córdoba, Av. Vélez Sarsfield 299 (5000), Córdoba, Argentina*

[3] *Department of Geological Sciences, Indiana University, 1005 East Tenth Street, Bloomington, IN 47405, USA*

[4] *Departamento de Petrología y Geoquímica, Facultad de Ciencias Geológicas, Universidad Complutense, 28040 Madrid, Spain*

[*] *Corresponding author*

Copper minerals (chrysocolla >> dioptase >> plancheite > tenorite) plus barite and quartz occur in a small lens of granulite-grade calcite–dolomite marble near Saldán, Córdoba Province (central Argentina, 31º18′50.7″S, 64º19′50.0″W). The mineralization is hosted in fractures (striking N30ºE and dipping 78ºW) that were widened by dissolution.

Chrysocolla mainly fills fractures. It has variable H_2O contents but the Cu:Si ratio is always close to 1 : 1. Plancheite forms compact fissure fillings and aggregates of interlocking spherules. Copper is partially replaced by Mg (up to 2.22 wt. % MgO), with small amounts of Na, K, Ca, Al and Fe also present. Dioptase occurs as prismatic crystals dominated by {10$\bar{1}$0} and {11$\bar{2}$1} that can reach over 2 cm in length, and also as granular fracture fillings. Unit-cell parameters are *a* 14.5719(6), *c* 7.7799(3) Å, *V* 1430.7(1) Å^3; refractive indices are ε = 1.707(3), ω = 1.656(3), with an anomalous small 2V. Magnesium (up to 0.15 wt. % MgO) is the only significant substituent. Yellow barite crystals tabular on {001} contain traces of Sr. Quartz occurs rarely, as drusy linings. A few cases of botryoidal, opal-like quartz crusts are known. Tenorite forms dark brown masses and stringers included in marble. Very scarce grains of copper sulfides (anilite altering to spionkopite and covellite along rims and cracks) are found scattered in the marble. Copper is partially replaced by Bi (≤0.15 wt. % Bi) and Pb (≤0.16 wt. % Pb). Malachite and brochantite are alteration products of sulfides.

Fluid inclusion studies indicate that the minerals precipitated from a single-phase fluid initially at a temperature above 300 ºC that cooled to *c.* 220 ºC. Salinity was very low, 0 to 2 wt. % NaCl eq. Isotopic analyses of calcite give $\delta^{13}C$ values of 0.4–0.9 ‰ PDB and $\delta^{18}O$ values of 17.1–15.1 ‰ VSMOW, coincident with the isotopic signature of the regional marbles. Calculated values of $\delta^{18}O$ for water in isotopic equilibrium with calcite fall into with the Metamorphic Water Box. The $\delta^{34}S$ values of barite are 3.6–4.6 ‰ CDT.

The mineralization possibly precipitated from fluids of meteoric origin that suffered an oxygen isotope shift due to a very low water/rock ratio. The sulfur source could have been sedimentary or igneous sulfides, or a mixture from two different sources (such as heavy seawater-derived sulfur and light sedimentary sulfides), but not exclusively seawater. Copper was probably scavenged from accessory sulfides scattered in barren marble or orthoamphibolite. The heat source remains unknown.

Keywords: dioptase, chrysocolla, plancheite, meteoric fluid, stable isotopes, fluid inclusions
Received: 13 May 2011; accepted: 27 September 2011; handling editor: S. Mills

1. Introduction

The interplay of processes acting on an oxidizing orebody can produce a vast array of secondary species, depending mostly on chemical factors such as pH, Eh and availability and activity of cations and anions in the solutions. Where copper is present in the primary minerals (usually sulfides), malachite and azurite are the most common secondary Cu-minerals. However, hydroxy-chlorides, sulfates, arsenates, phosphates, vanadates and silicates may be locally common and even of economic importance.

Dioptase, ideally $Cu_6(Si_6O_{18})\cdot 6H_2O$, is a cyclosilicate originally discovered in Altyn-Tyube (Altyn-Tube) deposit, Kirghiz Steppes, Karagandy Province, central Kazakhstan. René Hauy (1798) first realized that the crystals considered emerald were in fact a different species. Even though it is compositionally similar to chrysocolla, dioptase is much scarcer, indicating that the conditions leading to its precipitation are more restricted. Notably, in a number of the localities where dioptase is relatively abundant and where it forms the largest crystals, it occurs associated to dolomite (± calcite) (e.g. Markham 1959; Cook 2003; Walstrom 2006), suggesting that carbonate-rich environments are favorable for dioptase crystallization. In addition to the type locality, the most famous finds of this type were made in Africa,

especially at the Tsumeb mine in Namibia (Cook 2002; Cook and Nicolson 2002). As noted by these authors, species directly associated to dioptase tend to be few, even in deposits well-known for their mineralogical diversity; other Cu silicates (chrysocolla and plancheite), carbonates (malachite, calcite, dolomite and azurite) and quartz are among the most frequent. Pseudomorphs of plancheite after dioptase were also reported (Williams 1962; Vochten et al. 2005).

An occurrence of Cu-bearing minerals is found in marble near the town of Dumesnil, Córdoba Province (central Argentina). In spite of being volumetrically very small, this locality produced some fine crystals of dioptase. We present here a description of the geology and mineralogy, complemented by fluid inclusion and stable isotope data, to infer the origin of this mineralization.

2. Location and historical background

The occurrence is located in an area known as Mal Paso, between the towns of Dumesnil and Saldán (but closer to the second one), in Colón Department, Córdoba Province, central Argentina (31°18′50.7″S, 64°19′50.0″W) (Fig. 1).

Extensive marble mining for use in the cement industry has formerly taken place in this area. Nowadays a

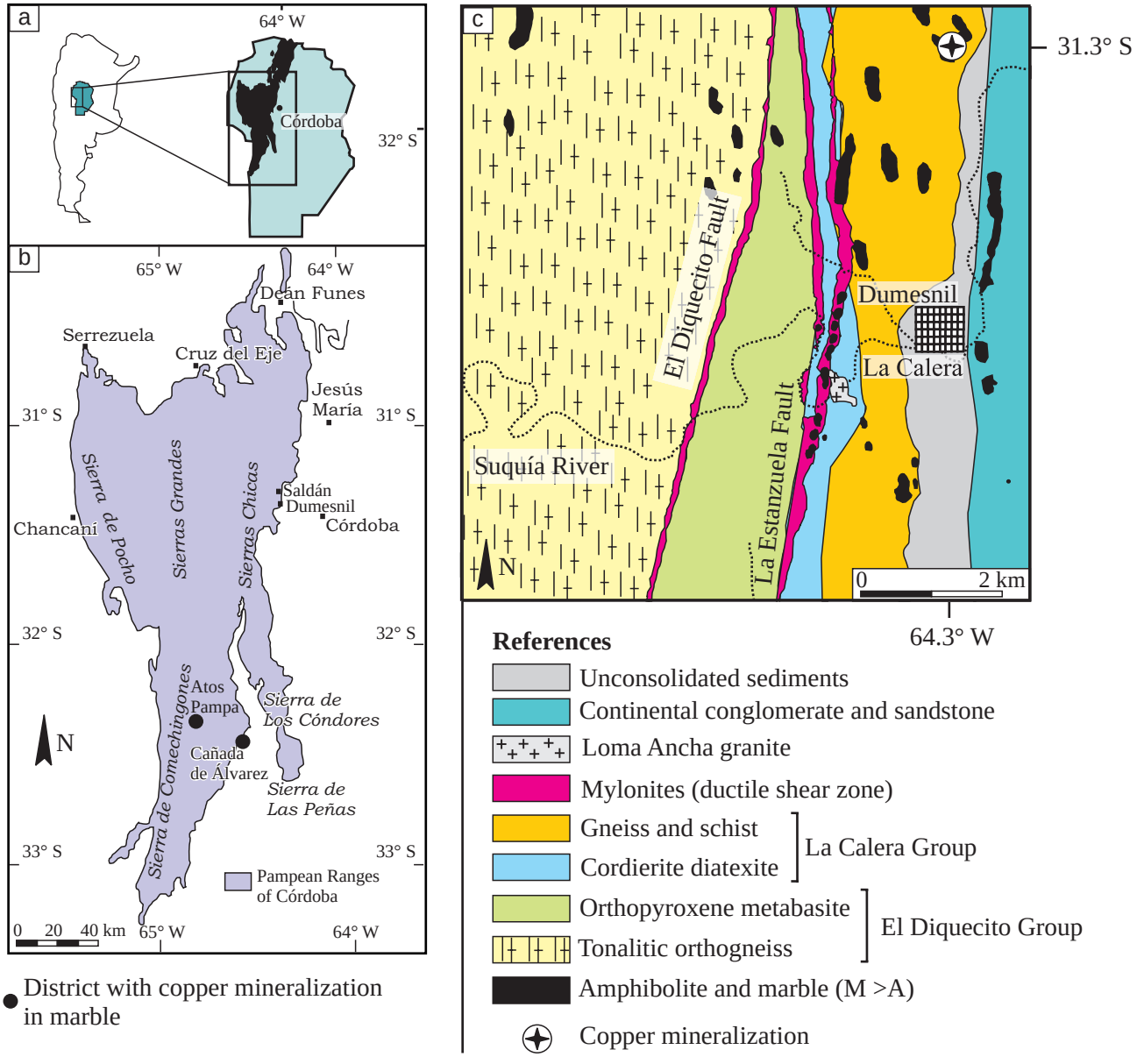

Fig. 1a Position of the Córdoba Province in Argentina (left) and Ranges (Sierras) of Córdoba (black) in the Córdoba Province (right). **b** – Sketch of the Ranges of Córdoba, showing two districts with copper mineralization in marble. **c** – Geological map of the studied area.

renewed interest in crushed stone for building purposes has led to reactivation of some old quarries and opening of new operations that exploit amphibolite and gneiss.

The first report of dioptase from the quarry of "Mal Paso" was made by Olsacher (1938), who mentioned that it was found as aggregates of anhedral (rarely euhedral) crystals in marble, up to 5 mm long and 1 mm wide. Gay et al. (1975) mentioned in a footnote that the *copper seams* [verbatim] in Mal Paso are 'very well known for the existence of dioptase'. Using X-ray diffraction, they identified plancheite. The next reference to dioptase was made by Angelelli et al. (1983), who presented a chemical analysis and a crystal drawing. Finally, Poklepovic et al. (2001) wrote a summary of the occurrence and gave data about fluid inclusions in dioptase.

After its discovery, this quarry has been owned successively by several individuals, who exploited it intermittently for dioptase specimens. For a period of time the quarry was given the name Esperanza (Hope). Mining progressed from two opposite sides, leaving an increasingly thinner wall between the two fronts. Most of the mining has been made in a rather primitive fashion, with picks and barrels.

3. Experimental techniques

X-ray powder diffraction patterns (XRPDP) were measured with a PANalytical X'Pert Pro diffractometer using CuK_α radiation obtained at 40 kV and 40 mA. Unit-cell dimensions were refined by full-profile fitting using the Le Bail method (Le Bail et al. 1988) as implemented by FullProf 2008 software (Roisnel and Rodríguez-Carvajal 2001). Reported standard deviations have already been multiplied by a correction factor (SCOR) to compensate for serial correlation (Bérar and Lennan 1991).

Whole-rock chemical analyses were performed using X-ray fluorescence (Rigaku RIX2000 spectrometer, wavelength-dispersive mode, Rh anode operated at 60 kV and 80 mA) at the Instituto de Geología y Minería (Universidad Nacional de Jujuy, Argentina). Major and minor elements were determined after fusion of the sample using Li borates. Trace elements were measured on pressed pellets.

Electron microprobe analyses (WDS mode) were carried out using a JEOL JXA 8900M microprobe at the Centro de Microscopía Luis Brú (Universidad Complutense de Madrid, Spain – UC) and a CAMECA SX-50 microprobe at the Brigham Young University (Utah, USA – BYU). Standards used for silicates (15 kV, 20 nA, 5 μm beam diameter, K_α lines) at UC were albite (Si, Na), sillimanite (Al), almandine (Fe, Mn), kaersutite (Ti, Mg, Ca), microcline (K), gahnite (Zn) and chalcopyrite (Cu). Counts were acquired for 10 s at the peak at 5 s at each background position. For sulfides we used 20 kV, 50 nA, a beam diameter of 2 to 5 μm and the same count times as for silicates. The lines and standards were as follows: L_α lines for Ag (pure Ag), As (AsGa), Pb (galena), Sb (GaSb), and Bi (BiTe), and K_α lines for Co, Ni, Cr (FeNiCoCr alloy), Ca (kaersutite), Fe and Mn (almandine), S and Cu (chalcopyrite), and Zn (gahnite). Instrumental parameters used at BYU for silicates were 10 nA, 15 kV, beam diameter 10 μm, 20 s count time on peak and 10 s at each side. Only K_α lines were used. Standards included MgO (Mg), anorthite (Al), chalcopyrite (Cu), orthoclase (Si), wollastonite (Ca), titanite (Ti), spessartine (Mn) and fayalite (Fe). Data were corrected using the PAP routine (Pouchou and Pichoir 1985) (CAMECA) or the ZAF algorithm (JEOL). Reported detection limits indicated in the respective tables of mineral analyses or given in the text are at a 2σ level, based on counting statistics. The H_2O content in dioptase was determined by loss on ignition at 1000 ºC for 10 hours. All mineral abbreviations are after Whitney and Evans (2010).

Backscattered electron images and energy-dispersive spectroscopy (EDS) spectra were acquired using an Amray scanning electron microscope equipped with an EDS system which detects elements with $Z \geq 11$ (Na), housed at the Earth and Environmental Sciences Department of the University of New Orleans (USA). Refractive indices were measured using single grains by immersion in Cargille oils.

Data from the study on fluid inclusions are summarized from Poklepovic et al. (2001). We inform here about the experimental conditions, which were not reported in that publication. Microthermometric runs were performed in a Fluid Inc. heating-freezing stage, calibrated with synthetic standards. The instrumental precision is ±0.1 C between –56.6 ºC and 660.4 ºC. Doubly polished sections ≤ 300 μm thick were used for microthermometric determinations. Measured data were processed with FLINCOR software (Brown 1989).

Two calcite and two barite samples were selected to evaluate O, C and S stable isotope data. $\delta^{18}O$ and $\delta^{13}C$ values were collected from calcite and $\delta^{34}S$ from barite. The CO_2 from vugs-filling calcite was extracted following the technique of Rosenbaum and Sheppard (1986) after overnight reaction with 100 % phosphoric acid at 50 ºC. Sulfur dioxide from barite was extracted by combustion, using a continuous continuous-flow methodology in an elemental analyzer. Barite NBS-127 (from seawater) was used as a standard.

All isotope ratios were measured on a Finnigan MAT 252 mass spectrometer; isotopic ratios were standardized to VSMOW (O), PDB (C) and CDT (S). Samples were run at the Stable Isotope Lab, Department of Geological Sciences, Indiana University at Bloomington, USA.

4. Regional geology

The Sierras de Córdoba, part of the Sierras Pampeanas (Pampean Ranges) in central Argentina, are composed of several north–south trending blocks that were lifted and tilted during the Andean orogeny (Tertiary) (Fig. 1a–b). There are three lithological belts that run along the mountain chains, separated by tectonic contacts: a western domain of low-grade metapelites, an eastern zone of medium-pressure granulite-facies metamorphic rocks derived from sedimentary and igneous protoliths, and an intermediate zone of middle to high amphibolite facies (Baldo et al. 1996a, b and references therein). Marble is much more abundant in the eastern than in the remaining two belts.

In the study area, located in the range known as Sierras Chicas and belonging to the eastern belt as listed above, two lithological domains have been recognized, separated by north-trending faults marked by intense mylonitization (Fig. 1c); the metamorphic grade increases eastwards (Gordillo and Lencinas 1979; Baldo et al. 1996a, b; Rapela et al. 1998). The La Calera Group, where the copper mineralization is located, is composed of Grt–Sil–Crd meta- to diatexites, along with subordinate gneisses, amphibolites and diopside marbles. Refractory enclaves of quartz, metaquartzite, amphibolites and orthopyroxene metabasites occur within the migmatites (Baldo et al. 1996a, b). The El Diquecito Group consists of two assemblages separated by the El Diquecito Fault. Tonalitic orthogneisses interlayered with minor high-grade paragneisses (Sil + Grt + Kfs) and lenses of marble and amphibolites dominate to the west of the fault. A much more complex sequence crops out east of the fault, with Opx–Grt metabasites, tonalitic orthogneisses and metasedimentary rocks (Sil + Grt gneisses and migmatites). Amphibolites have an N-MORB signature which, when coupled with positive ε_{Nd} values, strongly indicates that they represent relicts of the original oceanic crust (Rapela et al. 1998).

Baldo et al. (1996a, b) and Rapela et al. (1998) have demonstrated that this area has undergone at least 3 metamorphic events, which they called M_1, M_2 and M_3. Highest grade (granulite-facies) conditions were reached during M_2. Two samples of migmatite from La Calera Group gave P = 5.7 ± 0.4 kbar and T = 820 ± 25 ºC, and P = 6.3 ± 1 kbar and T = 820 ± 60 °C (Rapela et al. 1998). High-grade metamorphism related to anatexis has been dated by SHRIMP on monazite from the same paragenetic association at 522 ± 8 Ma ($^{206}Pb/^{238}U$) or 534 ± 7 Ma ($^{208}Pb/^{232}Th$) (Rapela et al. 1998). Somewhat higher pressure was calculated for a metabasite from El Diquecito Group, yielding P = 8.6 ± 0.8 kbar and T = 810 ± 50 °C for the M_2 event (Rapela et al. 1998). Conditions during the retrograde M_3 event were estimated at 4 ± 0.5 kbar and 715 ± 15 ºC (Baldo et al. 1996a).

Unmetamorphosed igneous rocks are scarce. The main body is the Loma Ancha muscovite granite, a small (less than 1 km along the longest axis) pluton. Peraluminous, barren or poorly mineralized (beryl-bearing) pegmatites reaching a few tens of meters in length with very simple mineralogy together with tonalitic dikes are scattered in all three metamorphic groups.

Cretaceous clastic rocks (conglomerates and sandstones) of continental origin cover discontinuously some sectors at the eastern flank of the Sierras Chicas.

5. Results

5.1. Geology of the mineralized area

5.1.1. The host rocks

The marble body that hosts the copper mineralization strikes N 157º E and dips 54º W, and it is composed of alternating reddish and whitish marble, sometimes with conspicuous bluish staining due to chrysocolla. Nine marble samples, differentiated by color and mineralogical variations, were extracted along a SE–NW profile (Fig. 2 and Tab. 1). Major rock-forming minerals are calcite and dolomite, defining a granoblastic texture with fine to coarse grain size. Macroscopic color ranges from reddish to white; in thin section carbonates are cloudy to clear. Minor phases are graphite, phlogopite and apatite, while lizardite and possibly tremolite are retrograde.

Graphite is very common as isolated scales and foliated masses up to 1 cm long, and also as inclusions in phlogopite (Fig. 3a–e). X-ray diffraction shows that it is the 2*H* polytype, with d_{002} ranging from 3.349 to 3.339 Å, indicating a near-maximum degree of order (Luque et al. 1998). The 3*R* polytype has not been detected.

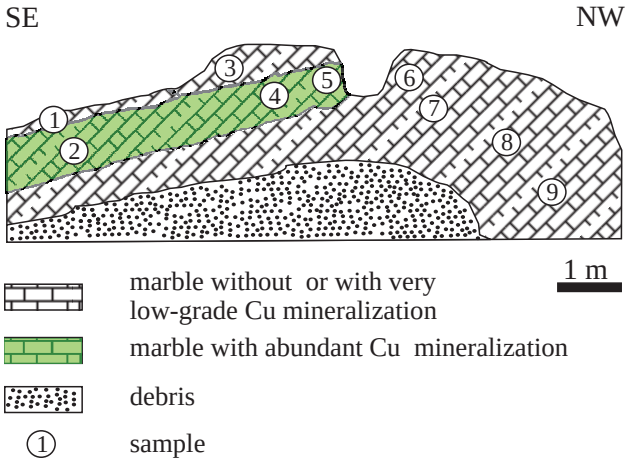

Fig. 2 Sketch of the quarry face showing the sampling spots as it appeared in 2005. Since then mining has drastically changed the topography.

Tab. 1 Marble samples representative of the Esperanza deposit

Sample	Average grain size	Color	Mineralogy
M1	3 mm	reddish brown	Cal, Dol, Gr, Ap
M2	6 mm	greyish white	Cal, Dol, Gr, Ccl, Phl, plancheite
M3	5 mm	pale reddish to greyish	Cal, Dol, Gr, Phl, Ap, Lz
M4	5 mm	light reddish brown	Cal, Dol, Phl, Gr, Ap, Tr
M5	2 to 8 mm	greyish	Cal, Dol, Gr, Lz, Phl
M6	7 mm	greyish white with Lz accumulations	Cal, Dol, Phl, Lz, Gr, Ap
M7	9 mm	light reddish brown	Cal, Dol, Phl, Ap, Gr
M8	4 mm	greyish with Lz accumulations	Cal, Dol, Phl, Gr, Ap, Lz

See Fig. 2 for sample locations.
Abbreviations after Whitney and Evans (2010). Samples in bold are from the zones richest in dioptase.

Phlogopite forms tabular euhedral to subhedral crystals up to 4 mm long (Fig. 3a, d).

Apatite is very abundant in some samples, as reflected by whole-rock contents of up to 1.72 wt. % P_2O_5. It occurs as colorless rounded grains up to 3 mm across, criss-crossed by numerous fractures (Fig. 3b). A microprobe analysis shows that it contains 0.27 wt. % MgO, while Na, Fe, Al, Mn and Si are below their detection limits (<0.09 wt. % as oxides). Traces of Cl were detected by EDS analyses.

Lizardite-1*T* is very common, sometimes giving a pale green color to the marble in hand specimens. It seems to be much more abundant in white than in reddish marble. This phyllosilicate occurs as rounded aggregates up to 2 mm long, macroscopically pale green and colorless under plane polarized light in the microscope; they show the typical finely fibrous texture under crossed polarizers (Fig. 3c). Where lizardite-1*T* occurs in close proximity to altered sulfides, it has a green color. In these cases EDS

Tab. 2 Chemical composition of marble found at the Esperanza deposit

	M1	M2	M3	M4	M5	M6	M7	M8	M9
wt. %									
SiO_2	12.72	6.94	8.05	7.53	12.20	9.36	6.55	16.78	9.65
TiO_2	0.01	0.07	0.06	0.04	0.13	0.06	0.02	0.02	0.06
Al_2O_3	0.24	0.16	0.84	0.76	0.28	0.79	0.61	0.39	1.11
Fe_2O_3	0.45	0.08	0.22	0.08	0.09	0.25	0.17	0.13	0.23
MnO	0.08	0.01	0.02	0.04	0.01	0.01	0.02	0.01	0.01
MgO	9.24	22.15	13.94	5.40	16.04	20.34	15.84	17.93	12.37
CaO	42.86	30.51	38.81	49.27	33.14	31.42	38.66	32.80	39.50
CuO	0.01	1.90	0.80	0.41	1.87	0.71	0.10	1.21	0.25
Na_2O	0.07	0.00	0.03	0.29	0.00	0.24	0.04	0.02	0.02
K_2O	0.01	0.08	0.31	0.31	0.10	0.42	0.15	0.24	0.21
P_2O_5	0.11	0.23	1.72	0.25	0.46	1.10	0.39	1.51	1.20
LOI	32.53	38.18	34.60	35.96	38.48	36.53	35.78	31.94	34.54
Total	98.33	100.31	99.40	100.34	102.80	101.23	98.33	102.98	99.15
ppm									
Ba	<20	<20	88	71	19	196	20	40	35
Nb	1	1	1	2	1	2	1	1	2
Zr	4	2	13	17	6	9	19	4	7
Y	8	7	11	9	8	9	8	5	9
Sr	101	40	57	90	55	58	73	82	60
Rb	3	4	7	5	3	11	5	6	6
Ni	18	24	22	17	27	23	20	21	20
Cr	4	<3	<3	<3	<3	3	<3	<3	<3
Th	<1	<1	2	2	<1	<1	<1	<1	<1
U	<1	3	2	<1	14	2	<1	4	<1
Cu	40	15213	6356	3260	14930	5704	776	9703	1967
Pb	4	29	11	13	89	65	22	93	7
Zn	12	15	8	5	23	9	5	10	16
Sn	<1	3.8	<1	<1	<1	2	<1	<1	<1

See Fig. 2 for sample locations.
Below detection limits: Ag (<10 ppm), Co (<5 ppm) and Hf (<10 ppm). Note that Cu appears twice, expressed as oxide (wt. %) and in an elemental form (ppm). Sample M9, not included in Tab. 1, is a reddish marble that extends from the deposit outwards.

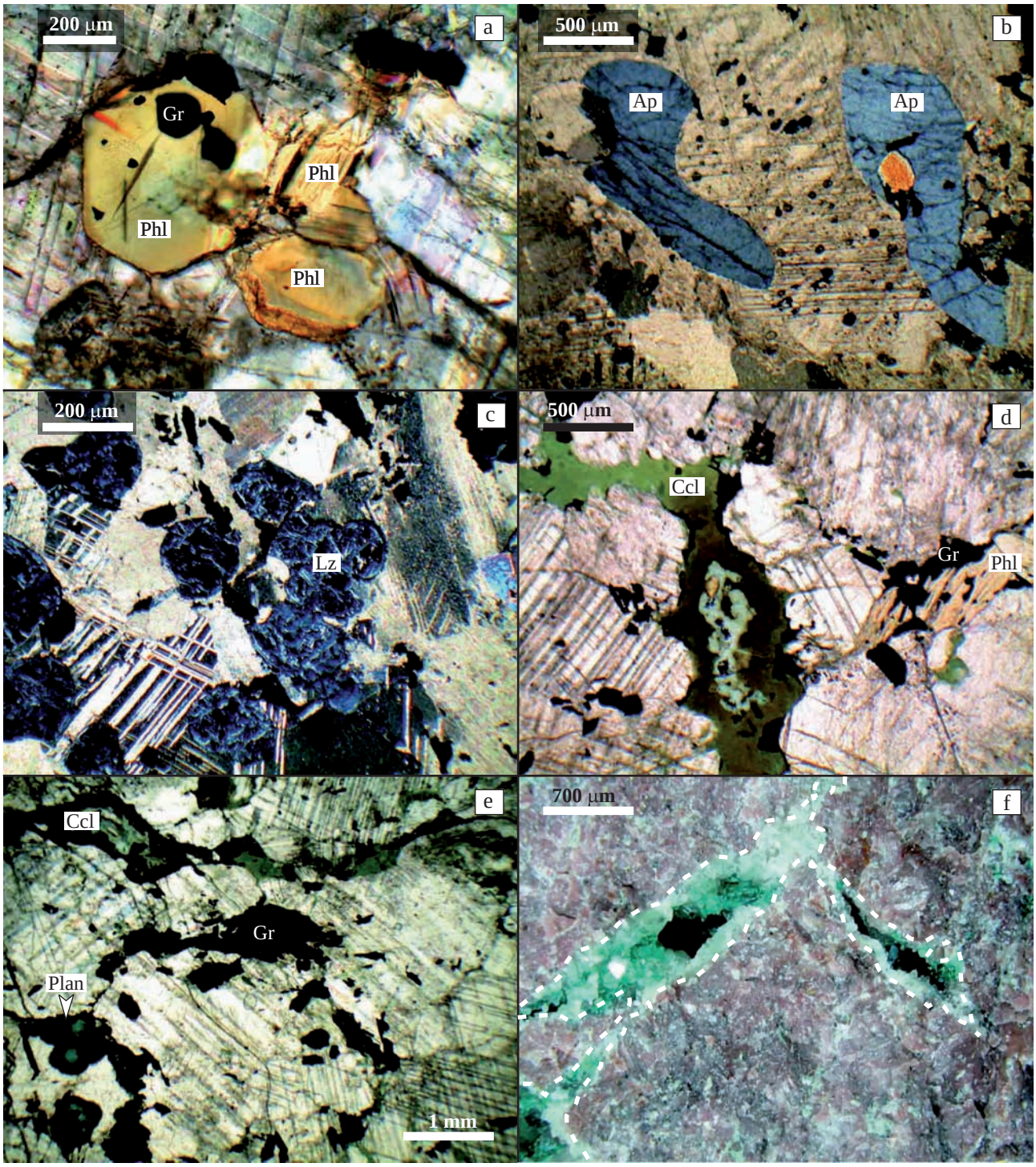

Fig. 3 Photomicrographs [in crossed polars, **a** to **e**] and photograph of the marble hosting the mineralization [**f**]. **a –** Phlogopite crystals with graphite inclusions. **b –** Two apatite blasts in carbonate. **c –** Lizardite-1*T* as a retrograde product after forsterite. **d –** Fissure filled by banded chrysocolla. The marble was partially dissolved but graphite flakes are not soluble and remain attached to the walls of the fissure. **e –** Fissures filled by banded chrysocolla and spherules of plancheite (Plan). **f –** Photograph of fissures in marble mineralized with dioptase and calcite. The dashed line marks the borders of the fissures.

spectra show small amounts of Cu, although it is not clear whether this element is somehow incorporated within the lizardite structure or whether it is present as submicroscopic inclusions of some other phase. The shape and texture indicate that it is a retrogression product of forsterite, of which no relics remain.

Whole-rock analyses of the marbles appear in Tab. 2. Strongly mineralized samples were not analyzed, but the

pervasive chrysocolla veining cannot be excluded, leading to high Cu values even in samples taken from areas more than 10 m away from the clearly Cu-rich zone. It can be seen that no other metal anomaly accompanies the Cu enrichment. The Mg content indicates that they are dolomitic marbles, which are common throughout the eastern flank of the Sierras Chicas between 31º 14′ and 31º 22′S. By contrast, calcitic compositions are dominant when the whole area is considered (Sfragulla et al. 1999).

5.1.2. Structural features

Copper-bearing minerals are concentrated in a lens-shaped body, approximately 15 m long, up to 3 m wide and 10 m deep. The marble lens is cut by faults on both the northern (where it is in contact with a garnet gneiss) and southern sides. The lens seems to pinch out towards the E, while the western side has been mined out and no records as for its shape and dimensions are available.

The mineralization (chrysocolla >> dioptase >> plancheite >> sulfides ≈ tenorite) is found in a network of fractures mainly hosted in white marble (Fig. 3d–e). Many fractures were widened by dissolution of carbonates. Non-soluble phases such as graphite are commonly seen at the contact between the marble and the hydrothermal minerals, but never as inclusions within these last phases (Fig. 3d). The mean strike of the fissure set mineralized with dioptase is N30º E dipping 78º W; a subordinate set has an attitude of N13º E/60º E. The main set is approximately coincident with one of the three main structural domains (termed D_3, with N20º E strike and a subvertical dip) of the Sierra de Córdoba, which is possibly of Late Ordovician or Silurian age (Dalla Salda 1984). However, there are many fine fractures, filled with dioptase or other Cu-bearing silicates, which do not belong to any of these sets. Some wider fissures (up to approximately 2 cm wide) are incompletely filled, with pinch-and-swell cavities lined with calcite and dioptase crystals (Fig. 3f). Calcite-filled fissures without Cu minerals are common throughout the deposit.

Effects of deformation are visible on outcrop scale as ductile bending of the marble layers, and also on thin-section scale by bent cleavage planes in carbonates and phlogopite. Mineralization preceded the latest faulting event, as evidenced by slickensides affecting copper silicates.

5.2. Mineralogy

Hydrothermal minerals include copper silicates (chrysocolla, plancheite and dioptase), tenorite, barite, quartz and calcite. The inferred paragenetic sequence appears in Fig. 4. The origin of sulfides is less clear, as discussed below. Malachite and brochantite occur as alteration products after sulfides.

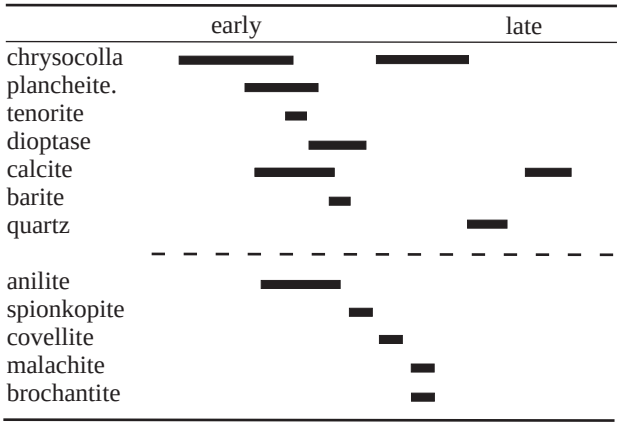

Fig. 4 Inferred paragenetic sequence. The dashed line separates two different paragenetic associations, the relationship between which is uncertain.

5.2.1. Chrysocolla

This is by far the most abundant copper mineral, occurring as thin fissure fillings in marble and encrustations over, or alternating with, calcite, and rarely with dioptase. Pseudomorphs of chrysocolla after an unknown mineral (most probably a carbonate with rhombohedral crystals of pseudocubic habit) were found (Fig. 5a).

This silicate is usually pale bluish green, opaque and lacks luster; more rarely it can have a dark blue green color and greasy luster. X-ray diagrams show that crystallinity (always poor, as is typical of chrysocolla), increases from the powdery to the porcelaneous variety.

From the chemical point of view, chrysocolla is very similar to dioptase, although it lacks long-range structural order. Chemical analyses of chrysocolla from Córdoba show very variable H_2O contents (assuming that the difference between the analytical total and 100 % corresponds to H_2O) but a Cu:Si ratio close to the expected 1:1 value. However, compared with dioptase, some elements (especially Mg, Al and Ca, and to a lesser degree Na and K) reach higher concentrations in chrysocolla (Tab. 3).

5.2.2. Plancheite

This silicate occurs as compact fissure fillings up to 3 mm thick, sometimes with fibrous structure. It also forms aggregates of interlocking spherules (up to 2 mm in diameter) with a radiating structure, lining fissure walls; the remaining space is filled by colorless calcite (Fig. 5b). Less often plancheite can be found as isolated spherules completely enclosed in chrysocolla. Color ranges from light to medium blue, rarely royal blue; some radial aggregates show concentric banding with a paler periphery. Massive plancheite is lusterless, but the surface of the radiating aggregates, after being exposed by dissolving the calcite with dilute HCl, has a silky luster.

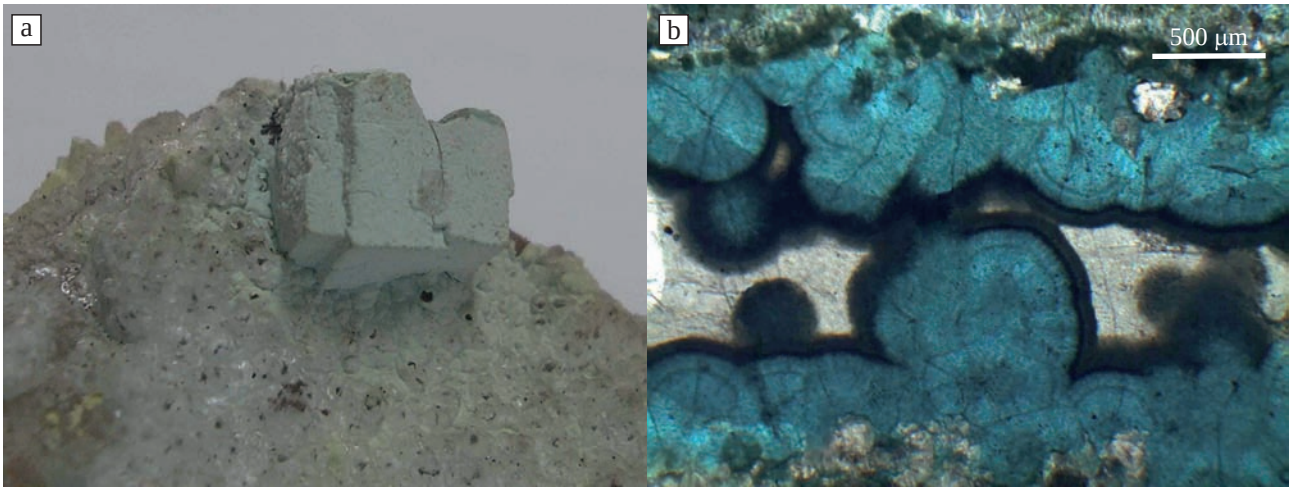

Fig. 5a – Pseudomorph of chrysocolla after an unknown phase (1 cm long), showing a pseudocubic morphology. **b –** Zoned plancheite spherules projecting into a calcite-filled fissure.

Tab. 3 Chemical composition of chrysocolla (wt. %)

	#12	#45	#46	#47	#48	#38-1
SiO_2	44.30	42.12	36.42	41.26	35.64	41.03
Al_2O_3	0.20	0.59	0.08	0.82	0.21	0.09
CuO	51.87	57.08	45.87	55.94	47.21	49.22
FeO	0.08	<0.03	<0.03	<0.03	<0.03	0.06
MgO	2.32	0.72	0.61	0.79	0.57	1.83
CaO	0.25	0.37	0.36	<0.03	0.33	0.29
Na_2O	0.22	<0.03	0.04	0.08	<0.03	n.m.
K_2O	0.43	<0.03	<0.03	<0.03	<0.03	n.m.
Total	99.67	100.88	83.38	98.89	83.96	92.52
apfu on a 18 O basis						
Si	6.044	5.838	6.018	5.829	5.911	6.030
Al	0.032	0.096	0.016	0.137	0.040	0.015
Cu	5.346	5.974	5.724	5.969	5.914	5.464
Fe	0.009	0.002	0.000	0.000	0.000	0.007
Mg	0.471	0.149	0.150	0.166	0.141	0.401
Ca	0.037	0.055	0.064	0.000	0.059	0.045
Na	0.057	0.000	0.013	0.021	0.000	
K	0.075	0.000	0.000	0.000	0.000	
Σ cations	12.071	12.114	11.985	12.122	12.065	11.962
M:T	0.99	1.04	0.99	1.03	1.03	0.98

M = Fe + Mg + Ca + Cu + Na + K; T = Si + Al. Measured on a JEOL instrument except for #38-1.
n.m.: not measured.

The X-ray powder diffraction patterns show very broad peaks, with a full width at half maximum value of 1.15º (2θ) for the 020 reflection at 8.43º (2θ). Unit-cell dimensions (refined in the space group *Pcnb*) are *a* 19.04(4), *b* 21.02(4), *c* 5.19(1) Å, *V* 2076(6) Å^3. The diffraction patterns match that of card 01-083-1241 of the Powder Diffraction Files of the Joint Committee on Powder Diffractions Standards (PDF-JCPDS).

The ideal chemical formula of plancheite is $Cu_8(Si_8O_{22})(OH)_4 \cdot H_2O$. Chemical analyses (Tab. 4) show that the Córdoba samples can contain important amounts of Mg (up to 2.22 wt. % MgO, i.e. up to 0.62 Mg *apfu*), with lesser Ca (up to 0.32 wt. % CaO), Al (up to 0.11 wt. % Al_2O_3), Fe (up to 0.06 wt. % FeO) and Mn (up to 0.08 wt. % MnO). Sodium (up to 0.23 wt. % Na_2O) and K (up to 0.43 wt. % K_2O) are also present. Titanium is below the detection limit (0.09 wt.% as TiO_2).

5.2.3. Dioptase

This copper silicate forms prismatic crystals that can reach over 20 mm long and 6 mm thick, with a typical length : width ratio of ~4. They occur included in calcite or growing in open fissures, isolated or forming divergent groups (Fig. 6a–d). Most crystals are morphologically simple, dominated by the {10$\bar{1}$0} prism terminated by {11$\bar{2}$1} rhombohedron, sometimes combined with other forms of minor development (Angelelli et al. 1983). Thin compact veins of granular dioptase are more common towards both sides of the mineralized outcrop. Dioptase is translucent to transparent, with a bright to dark green color and vitreous luster. Some crystals display an incipient alteration, turning opaque and with dull luster (Fig. 6e). As mentioned above, crystals are fragile due to the perfect cleavage on {10$\bar{1}$1}. X-ray diffraction data show excellent agreement with those reported in the card 01-072-1956 of the PDF-JCPDS; refined unit-cell parameters (in the space group $R\bar{3}$) are *a* 14.5719(6), *c* 7.7799(3) Å, *V* 1430.7(1) Å^3. In plane polarized light dioptase is intense green with no pleochroism; measured refractive indices are ω = 1.656(3), ε = 1.707(3) with a small anomalous

Tab. 4 Chemical composition of plancheite (wt. %)

	#38-2	#38-4	#38-5	#38-6	#A-a	#A-b	#B
SiO_2	43.31	42.72	42.93	43.31	43.41	43.46	44.08
Al_2O_3	0.04	0.04	0.05	0.04	0.09	0.09	0.11
FeO	0.06	<0.03	0.04	0.09	0.06	<0.05	<0.05
MnO	0.00	0.02	0.00	0.00	<0.06	<0.06	0.08
MgO	1.87	1.88	2.04	1.89	1.89	1.99	2.22
CaO	0.23	0.16	0.19	0.22	0.29	0.28	0.32
CuO	51.53	51.73	50.18	51.20	49.00	49.17	48.37
Na_2O	n.m.	n.m.	n.m.	n.m.	0.23	0.16	0.14
K_2O	n.m.	n.m.	n.m.	n.m.	0.43	0.32	0.41
H_2O calc	4.82	4.78	4.76	4.81	4.76	4.77	4.82
Total	101.86	101.33	100.19	101.56	100.16	100.24	100.55
apfu on a 24 O equivalent basis							
Si	8.076	8.037	8.105	8.090	8.193	8.182	8.226
Al	0.009	0.008	0.011	0.009	0.019	0.019	0.024
Fe	0.009	0.000	0.006	0.013	0.009	0.002	0.000
Mn	0.000	0.003	0.000	0.000	0.000	0.000	0.013
Mg	0.518	0.527	0.573	0.525	0.533	0.560	0.616
Ca	0.045	0.032	0.038	0.044	0.058	0.056	0.065
Cu	7.258	7.351	7.155	7.223	6.985	6.991	6.817
Na	–	–	–	–	0.085	0.058	0.050
K	–	–	–	–	0.102	0.077	0.098
H calc	6.000	6.000	6.000	6.000	6.000	6.000	6.000
Σ cations*	15.915	15.958	15.888	15.904	15.984	15.945	15.909

Measured on a CAMECA instrument except for #A-a, #A-b and #B. H_2O content calculated by stoichiometry. Zinc was found to be below about 1000 ppm (2σ) in all cases.
n.m.: not measured.
*Calculated H *apfu* not included in the sum of cations.

2V. Refractive indices fall within the range given by Anthony et al. (2001): 1.652–1.658 for ω and 1.704–1.710 for ε.

Even though dioptase from other localities may show minor but significant substitutions at the Cu site, mainly Ca, Mg and Zn (e.g., Pauliš et al. 2006), electron microprobe analyses (Tab. 5) show that the dioptase from Córdoba has an almost stoichiometric composition, with only small amounts of Mg (0.06–0.15 wt. % MgO, 0.01–0.03 *apfu* Mg). Iron and Al are present in quantities close to, or below, the detection limit (≤ 0.03 wt. % of their oxides), whereas Mn, Ca, Ti and Zn are always below their respective detection limits (300–1000 ppm, depending on the element). No systematic changes were observed between cores and rims of the crystals. The slight deviations from the stoichiometric values (ideally 38.93 wt. % SiO_2, 49.51 wt. % CuO) are considered to be an artifact, probably because chal-

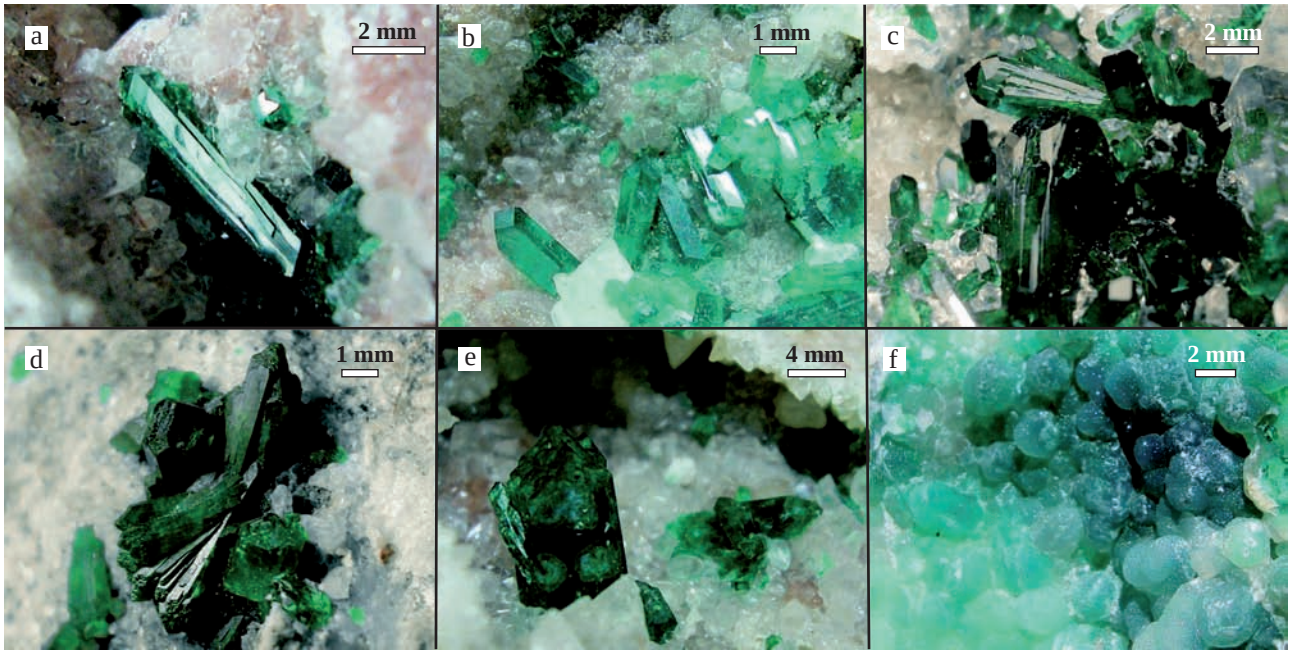

Fig. 6 Dioptase crystals. **a** to **d** – Dioptase crystals growing on calcite. **e** – Dioptase with altered surface, evidenced by concentric rings. **f** – Crust of calcite microcrystals overgrowing dioptase.

Tab. 5 Chemical composition of dioptase (wt. %)

	#39-1-b	#39-1-ia	#39-1-ib	#39-1-c	#50	#51
SiO_2	38.87	38.76	38.67	38.78	39.61	40.65
Al_2O_3	0.03	0.03	<0.03	0.03	<0.03	0.06
FeO	<0.03	0.04	0.05	0.03	0.03	<0.03
CuO	51.01	51.04	52.05	52.49	49.99	51.50
MgO	0.24	0.30	0.17	0.13	0.15	0.06
H_2O meas	11.91	11.91	11.91	11.91	11.91	11.91
Total	102.06	102.08	102.85	103.37	101.69	104.18
apfu on a 18 O basis						
Si	5.996	5.982	5.951	5.941	6.081	6.077
Al	0.006	0.005	0.000	0.006	0.000	0.011
Fe	0.000	0.005	0.006	0.003	0.004	0.000
Cu	5.943	5.950	6.050	6.074	5.797	5.815
Mg	0.055	0.070	0.038	0.029	0.034	0.013
H	6.130	6.133	6.116	6.088	6.100	5.941
Σ cations	18.130	18.145	18.161	18.141	18.016	17.857

Measured on a CAMECA instrument except for #50 and #51.

copyrite (instead of an oxygen-containing material) was used as a Cu standard or to the data reduction software. An analysis of dioptase from this quarry made using gravimetric methods was published by Angelelli et al. (1983), who reported 38.00 wt. % SiO_2, 50.40 wt. % CuO and 11.52 wt. % H_2O, total 99.92 wt. %. This corresponds to $Cu_{6.00}(Si_{6.07}O_{18})\cdot 6.07H_2O$.

5.2.4. Calcite

Among the hydrothermal minerals, calcite is the most abundant phase, forming scalenohedral or rhombohedral colorless, whitish or very pale yellow crystals up to 4 cm long and sometimes twinned on {0001}. Most often crystals show an incipient dissolution, giving them a somewhat greasy luster. Coarse-grained masses filling fissures are common throughout the deposit. A late generation of very fine grained, lusterless grayish calcite covers some surfaces in cavities, sometimes displaying a fine banding. It is most likely that this generation precipitated from percolating meteoric water and it is probably unrelated to the mineralization process.

5.2.5. Barite

Very rare barite occurs as groups of crystals of up to 9 mm long, tabular on {001} with smaller {100}, {011}, {110} and {111}. Color ranges from pale to bright yellow, often with concentric color zoning visible along [001]. Crystals are always implanted on calcite and rarely

Tab. 6 Electron microprobe analyses of sulfides (wt. %)

	anilite							covellite		spionkopite	
	#2	#8	#9	#10	#4	#5	#6	#3	#7	#1	#11
Bi	0.11	0.09	0.06	0.13	0.07	<0.05	0.07	0.08	0.15	0.13	0.08
S	22.26	22.54	22.35	22.49	22.49	21.84	22.40	33.51	33.72	24.17	25.16
Cd	<0.03	<0.03	<0.03	<0.03	<0.03	<0.03	<0.03	<0.03	0.03	<0.03	<0.03
Pb	0.08	0.09	0.10	0.12	0.09	0.12	0.11	0.16	0.15	0.06	0.13
Cu	76.71	77.13	76.82	76.74	75.60	76.41	76.53	65.38	64.61	68.73	67.52
Sb	0.05	0.10	0.07	0.06	0.04	0.05	0.04	0.05	0.03	0.06	0.06
Fe	<0.02	<0.02	<0.02	<0.02	0.03	<0.02	<0.02	0.05	<0.02	6.36	7.15
Ag	0.02	0.04	<0.02	0.03	0.02	<0.02	<0.02	0.06	<0.02	0.03	0.02
Total	99.23	99.98	99.40	99.57	98.34	98.42	99.14	99.28	98.69	99.55	100.12
apfu											
S	4.00	4.00	4.00	4.00	4.00	4.00	4.00	1.00	1.00	5.00	5.00
Bi	0.00	0.00	0.00	0.00	0.00	0.00	0.00	0.00	0.00	0.00	0.00
Cd	0.00	0.00	0.00	0.00	0.00	0.00	0.00	0.00	0.00	0.00	0.00
Pb	0.00	0.00	0.00	0.00	0.00	0.00	0.00	0.00	0.00	0.00	0.00
Cu	6.95	6.91	6.94	6.89	6.78	7.06	6.90	0.98	0.97	7.17	6.77
Sb	0.00	0.00	0.00	0.00	0.00	0.00	0.00	0.00	0.00	0.00	0.00
Fe	0.00	0.00	0.00	0.00	0.00	0.00	0.00	0.00	0.00	0.76	0.82
Ag	0.00	0.00	0.00	0.00	0.00	0.00	0.00	0.00	0.00	0.00	0.00
Σ cations	6.96	6.92	6.95	6.90	6.80	7.07	6.90	0.99	0.97	7.94	7.60
(Cu+Fe)/S	1.74	1.73	1.74	1.73	1.70	1.77	1.73	0.99	0.97	1.59	1.52

Formulae normalized on a basis of 4 (anilite), 1 (covellite) or 5 (spionkopite) sulfur atoms per formula unit.
Also sought for but not detected, with detection limits (2σ, in ppm): As (340), Co (260), Ni (260), Zn (520), Ca (120) and Mn (260). Analyses carried out by JEOL microprobe.

in contact with dioptase. Elements detected using EDS are major S and Ba, and trace amounts of Sr.

5.2.6. Tenorite

Dull, blackish brown masses and stringers included in marble were identified by X-ray diffraction as tenorite, with broad peaks indicative of very small crystallite size. Textural relations with copper silicates suggest that tenorite crystallized later, at least relative to plancheite and the first chrysocolla stage.

5.2.7. Copper sulfides; malachite and brochantite

Very scarce grains of copper sulfides are found as inclusions in the marble. Macroscopically they are grayish black with a thin dark blue rim. Electron microprobe analyses (Tab. 6) show that the core is composed of anilite, which is partly replaced by covellite and small amounts of spionkopite along the rims and cracks (Fig. 7). In addition to the essential structural constituents, sulfides contain traces of Bi (≤0.15 wt. %) and Pb (≤0.16 wt. %). Silver and Sb are present just above the detection limits (*c.* 250 ppm, at 2σ).

Fibrous masses of malachite and brochantite (both confirmed by powder XRD and EDS) occur partially surrounding the sulfide grains (Figs 7a–b).

Sulfides (and secondary malachite and brochantite) cannot be unequivocally inserted in the paragenetic sequence mentioned above, as they occur in a different micro-environment (granular marble, as opposed to fissure fillings) and do not display cross-cutting relationships with other copper minerals. The chrysocolla films surrounding and crossing some sulfides are an exception, but they could have a local origin and be unrelated to chrysocolla associated with dioptase and plancheite. At present it is not known whether sulfides were deposited during the same mineralizing event or they pre-dated the silica-rich minerals.

5.3. Fluid inclusions

The results of a fluid inclusions study were briefly summarized by Poklepovic et al. (2001), and are presented in full here. The study was aimed at obtaining insight into the temperature and fluid composition that prevailed during the precipitation of copper minerals. Therefore, only primary inclusions were measured; a careful search revealed useful fluid inclusions only in dioptase.

Fluid inclusions occurring in sections representing five different crystals of dioptase are irregularly shaped and occur as clusters or isolated. The size of individual inclusions ranges from 11 to 25 μm. Fluid inclusions show two phases (L + V), with a degree of fill (*F*) of ~0.7. Fluid inclusions lack daughter crystals, but a few accidentally trapped opaque solids were seen in several cases. Homogenization temperatures (T_h) vary between 217 and 311 ºC, with a mean of 259 ºC (n = 33), whereas ice-melting temperatures (T_{mi}) range from –0.9 to 0.0 ºC (n = 27). No CO_2 was detected during the freezing runs. Calculated salinities are thus very low, from 0 to 2 wt. %

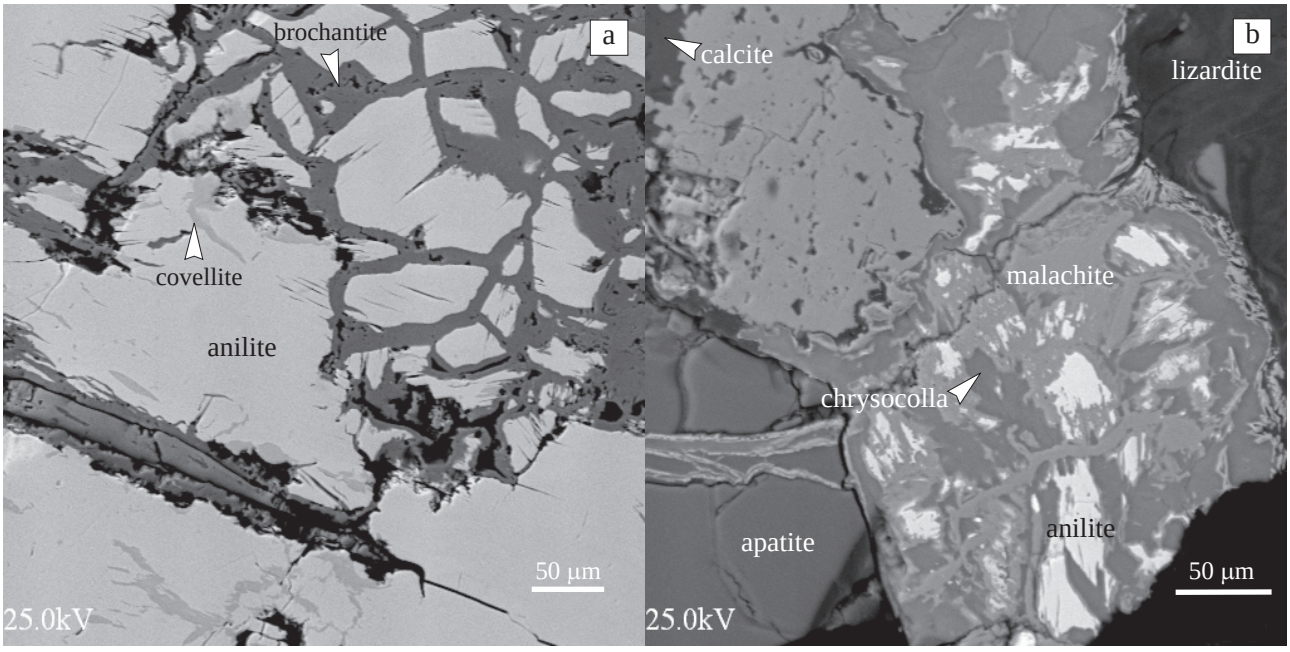

Fig. 7 Backscattered electron images of sulfides and their alteration products. **a** – Anilite relics with covellite along fissures, separated by a network of brochantite. **b** – Grain of anilite in marble, partially altered to malachite and chrysocolla.

NaCl equivalent (Fig. 8). The restricted compositional variation and approximately constant value of *F* imply that the hydrostatic pressure was larger than the vapor pressure, preventing boiling. Accordingly, no macroscopic evidence suggestive of boiling or extensional structures, such as breccias, calcite with bladed habit or infill textures, was observed. This means that the measured homogenization temperatures are in fact minimum values, but unfortunately no clues regarding confining pressure during dioptase precipitation were unraveled.

Gas-rich, irregular secondary inclusions are arranged along {11$\bar{2}$1} cleavage planes or fractures, becoming more abundant were these discontinuities intersect. Necking-down is widespread in secondary inclusions, with daughter crystals present in the fluid-rich portions. The wide and continuous variation of homogenization temperature combined with the narrow range in salinity (Fig. 8) is interpreted as reflecting a simple cooling path.

The examined calcite samples (at least 7 cleavage fragments taken from each of the two specimens used for isotopic analyses) have curved planes decorated by tiny (mostly ≤4 μm) fluid inclusions, clearly showing that they are sealed fractures. Although T_h were not measured, the high *F* values (estimated at above 0.95) suggest a low trapping temperature, possibly below 150 ºC. A few larger inclusions were seen in these planes; however, in addition to being of secondary origin, they show prominent necking-down features such as long, thin tapering tails and variable *F* values. No inclusions with textural features suggestive of a primary origin were found in either of these samples, or in a few other calcite specimens. The only examined barite crystal lacks fluid inclusions.

5.4. Analysis of stable isotopes

The two analyzed colorless, coarse-grained calcite samples occur in contact with dioptase and were taken from the central part of completely filled fissures. Some dioptase crystals occurring with calcite texturally similar to this display irregular surfaces where they are in contact with the carbonate, indicating precipitation simultaneous with calcite crystals. Therefore, we assume that the isotopic characteristics of the carbonate reflect those of the main mineralization event.

The two calcite samples are isotopically rather similar to each other (Tab. 7), and compare fairly well to $\delta^{13}C$ values of high-grade regional marbles that crop out in the vicinity. In the Michelotti quarries at La Calera town, the dolomitic–calcitic marble yielded a $\delta^{13}C$ value of 0.5 ‰ (± 0.1 ‰), and in the Ferreyra quarries at Malagueño, the $\delta^{13}C$ value of a calcitic marble was 0.9 ‰ (Panarello et al. 1980). The studied Esperanza quarry can be considered part of the Michelotti quarries from a regional geologic perspective, whereas the Malagueño quarries, located 15 km to the south, belong to the same metamorphic belt. Panarello et al. (1980) found a range from 4.6 to –1.4 ‰ $\delta^{13}C$ for a suite of Cambrian dolomitic and calcitic marbles representative of the easternmost range of the Sierras Pampeanas Orientales in Córdoba Province (including the Michelotti and Ferreyra quarries). The $\delta^{18}O$ compositions of these marbles were not measured by Panarello et al. (1980). Nevertheless, the $\delta^{18}O$ values of Cal–1 (17.1 ‰) and Cal–2 (15.1 ‰) plot well within the known ranges for metacarbonates from other regions of the Sierras Pampeanas Orientales. The Tab. 7 lists the different calculated values of $\delta^{18}O$ for water in isotopic equilibrium with calcite at 300 ºC and 250 ºC. Regardless of the chosen equation and temperature, all calculated H_2O isotopic compositions plot within the Metamorphic Water Box (Kerrich 1987). It should be remembered that isotopic values were calculated using the homogenization temperatures of fluid inclusions, which have not been pressure-corrected because of insufficient pressure constraints. Therefore, the trapping temperature is higher; this is why the results calculated using 300 ºC are probably closer

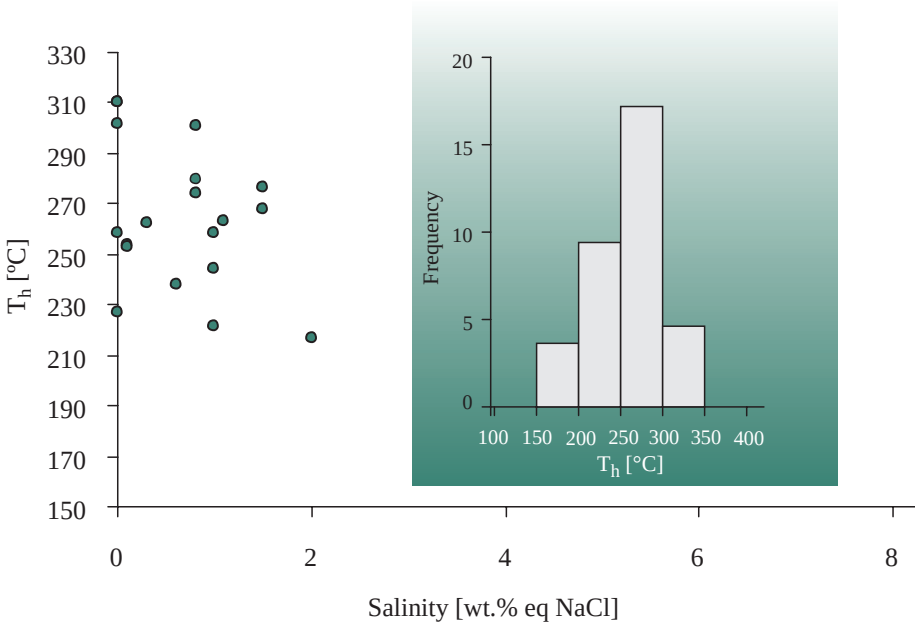

Fig. 8 Plot of salinity vs. temperature of homogenization (T_h) for fluid inclusions in dioptase. Inset: histogram showing the distribution of T_h.

Tab. 7 Isotopic analyses of calcite and calculated values for $\delta^{18}O_{H_2O}$ for water in equilibrium with calcite

Sample	$\delta^{13}C$ (‰)	$\delta^{18}O$ (‰)	Calculated values of $\delta^{18}O_{H_2O}$ for water in equilibrium with calcite at 300 ºC (‰)		
			O'Neil et al. (1969) and Friedman and O'Neil (1977)	Zheng (1999)	Kim and O'Neil (1997)
Cal-1	0.9	17.1	11.5	11.3	18.1
Cal-2	0.4	15.1	9.5	9.3	16.1
			Calculated values of $\delta^{18}O_{H_2O}$ for water in equilibrium with calcite at 250 ºC (‰)		
Cal-1			9.84	9.66	15.07
Cal-2			7.82	7.64	13.10

to the actual isotopic values of the fluid, even though the average T_h (not pressure-corrected) is 259 ºC.

Two $\delta^{34}S$ values recorded by barite from the Esperanza quarry fall within the range 3.6 to 4.6 ‰ CDT. Just a few samples of barite were found, and the very restricted position of this sulfate in the paragenetic sequence (see Fig. 4) suggests that the tight range of $\delta^{34}S$ values may indeed be representative of the Esperanza showing. Unfortunately, the copper sulfides also present are too scarce to be analyzed with the available techniques.

6. Discussion

As described above, the fluid that deposited copper silicates, calcite and barite was hot (with maximum temperature above 300 ºC, considering that a pressure correction to the measured T_h should be applied) and very dilute (0–2 wt. % eq. NaCl).

Such homogeneous, very low salinity is typical of fluids of meteoric origin (e.g., Richards and Spooner 1989; Seal and Rye 1993; Craw 1997; Bajnoczi et al. 2000; Moritz 2006; Fernández et al. 2008), although it is not unknown from other systems such as porphyry Cu (± Mo) deposits (e.g. Gammons and Williams-Jones 1997; Rusk and Reed 2008; Sillitoe 2010). However, in most of these latter cases, low-salinity fluids are found solely in one of several fluid inclusion assemblages, the others having higher salinities (e.g. Pudack et al. 2009). In addition to that, in many cases the meteoric water is indeed involved in these hydrothermal systems, this being one of the causes for the low-salinity fluids (e.g. Zhang et al. 1989). Fluids of metamorphic origin can also have low salinity, but they usually contain carbon compounds such as CO_2 or CH_4 (e.g., Naden and Shepherd 1989; Witt et al. 1997; Mishra and Pal 2008). These gases are also rather common in fluids of igneous origin. Given the absence of nearby intrusive centers (see below), and considering that the copper mineralization postdated the regional metamorphic peak, we prefer the hypothesis that the fluids responsible for the copper mineralization had a dominantly meteoric origin, consistent with their low salinity and absence of gases (detectable by freezing measurements) other than H_2O vapor. Additional stable isotope data are necessary to further constrain the fluid source. The isotopic signature closely concordant with the local marble can be explained by a very low water/rock ratio, which caused an oxygen isotope shift. The enclosing marble was most likely the source of Ca^{2+} and $(CO_3)^{2-}$ for calcite deposition, through dissolution–reprecipitation. Comparable isotopic compositions were calculated by Lira et al. (2008) for water in equilibrium with epidote and clinozoisite from retrograde skarns elsewhere in the Sierras Pampeanas Orientales of Córdoba Province. The heavy $\delta^{18}O_{H2O}$ and $\delta^{2}H_{H2O}$ computed from both epidote-group minerals were interpreted as reflecting the inherited isotope composition of the skarn garnet they replaced, which grew at the expense of metasedimentary protolithic phases.

Sulfur isotopic fractionation in hydrothermal ore deposits is a complex function of temperature, pH, fO_2, original isotopic composition and sulfur speciation (mainly SO_4^{2-} and H_2S) in the fluid (Ohmoto and Rye 1979). Fortunately, it has been shown that sulfur isotopic patterns are preserved during metamorphism (e.g., Cook and Hoefs 1997 and references therein; Alirezaei and Cameron 2001; Russell et al. 2010) and that the direct oxidation of sulfide to sulfate provides only minimum fractionation (e.g. Canfield 2001).

An origin of sulfur exclusively from seawater can be discarded, as shown by curve depicting the secular variations of $\delta^{34}S$ in seawater sulfate (Seal 2006). This precludes some common sulfur sources such as evaporite minerals, phosphate-bound sulfate, carbonate-associated sulfate and marine barite, as all these would be expected to show the seawater signature (Turchyn et al. 2009).

Considering the geological context, some of the possible sources of sulfur closest to the studied copper mineralization are sulfides dispersed in the marble itself, in calc-silicates interleaved in the metamorphic sequence, and as accessory phases in ortho-amphibolites.

Sedimentary sulfides display a wide range of $\delta^{34}S$ values, from less than –50 to over +20 ‰, although most have negative values due to Rayleigh fractionation of sulfur isotopes during the diagenetic bacterial sulfate reduction (Seal 2006). Unfortunately there are no data on the sulfur isotopic composition of marble-hosted sulfides from the deposit or, indeed, the rest of the Sierras Pampeanas Orientales.

Calc-silicate rocks are the result of regional metamorphism of mixed clastic and carbonate protoliths, without

appreciable elemental input from an external source. Therefore, any sulfide occurring in these rocks should share the isotopic characteristics discussed above for the marble protoliths.

Any evidence of magmatic activity that could have been a direct source of hydrothermal fluids and elements is lacking in the area. However, nearby ortho-amphibolite bodies could host sulfides with magmatic-like $\delta^{34}S$ (mostly 0 ± 5 ‰), which on dissolution would provide a suitable S source for barite. A high SO_4^{2-}/H_2S ratio is inferred from the absence of sulfides in the paragenetic association at the Esperanza showing. Under these conditions, barite precipitated at 200 ºC from a fluid with $\delta^{34}S_{\Sigma S}$ = 0 ‰ would have a $\delta^{34}S$ value of +3.2 (Rye and Ohmoto 1974), comparable to those found in this work.

Other possibility that should be considered is the fact that the $\delta^{34}S$ value of *c.* +4.1 may have resulted from the mixing of solutions carrying contrasting $\delta^{34}S$ signatures, such as a light source derived from oxidation of sedimentary sulfides and a heavy one from seawater-related sulfate. On the other hand, the two closely comparable values of $\delta^{34}S$ in barite available for the deposit do not provide further support for such a mixing hypothesis.

A related issue is the source of copper. The same candidates mentioned above as possible sources of sulfur (namely sulfides scattered in the marble, in calc-silicate rocks or in amphibolite) could have conceivably released copper as well.

Copper mineralization hosted in dolomitic marbles is known from different deposits (none of economical significance) and showings scattered in the Sierras Pampeanas of Córdoba, the most relevant localities being the Cañada de Álvarez and Atos Pampa districts (Fig. 1b). Primary mineralization consists mainly of chalcocite, with traces of chalcopyrite, pyrrhotite, bornite, digenite, gold, and possibly wittichenite and silver. Malachite, dioptase and pseudomalachite are found among the Cu-bearing secondary species (Brodtkorb et al. 1981). As yet, there is no consensus regarding the source of the copper. Some researchers have postulated an origin related to bio-mineralization by algae, under reducing conditions in a restricted marine basin (Brodtkorb et al. 1981; Mutti et al. 1998). However, the Cu-rich layers are locally discordant to the marble foliation, implying that if the biogenic origin could be proven then there has been at least some local hydrothermal remobilization. As an alternative, Mutti and Di Marco (1999) suggested that the intercalations of tholeiitic metabasalts with MORB signature within the carbonate sequence support a hypothesis that copper could have been related to submarine exhalations, and that the deposit could be better classified as a SEDEX-type. However, more data are needed to provide additional support to either of the two competing hypotheses.

Another possible source are amphibolites, which are known to be genetically related to very small deposits found along the Sierras of Córdoba. The metallic association is Cu + Fe (± Zn, Au, Ag, Co), represented by chalcopyrite and magnetite with varying amounts of pyrite, pyrrhotite, hematite, bornite, sphalerite, silver, carrolite, and ilmenite. Tetrahedrite and gold are rare accessories (Mutti and Di Marco 1999 and references therein). The copper content of non-mineralized amphibolites is up to 240 ppm, although most values are very low, close to zero (Daziano 2004).

No metallic anomaly such as any of those mentioned above is found within a reasonable distance (tens of km) of the Esperanza showing. Therefore, and unless a buried or eroded source is invoked, the copper should have been released from copper (± other metals) sulfide grains present as accessory phases in the barren marble or amphibolite.

The absence of copper carbonates could be explained by the abundance of Ca^{2+} in the mineralizing solutions. Under these conditions, the solubility product of calcite would be reached before that of copper carbonates. Also, a low ratio of $P_{CO_2}/a\mathrm{SiO}_2$ should stabilize chrysocolla instead of malachite (see Crane et al. 2001). Malachite is found to be restricted to the immediate surroundings of altered sulfides, where *a*Cu was high enough to stabilize this mineral. The sequence plancheite → dioptase → quartz involves an increase in $a\mathrm{SiO}_2/a\mathrm{Cu}$. Experiments have shown that the conditions leading to chrysocolla precipitation are low Cu activity, SiO_2 concentration below that yielded by equilibration with amorphous SiO_2, and medium to high pH (5–9) (Newberg 1967; Yates et al. 1998). For solutions at the pH range expected in systems buffered by calcite and CO_2 (between 9.95 and 8.31, but usually closer to the lower value; Sato 1960) that are very dilute and with low Cl contents, the dominant Cu species is $Cu(OH)_2^0$, followed successively by $Cu(OH)^+$, Cu^{2+} and $Cu_2(OH)_2^{2+}$ (Yates et al. 1998).

The identity of primary sulfides in the marble remains unknown, as anilite is usually the product of copper leaching of a precursor mineral (e.g., Hatert 2005), but no relics of such a putative primary sulfide were detected. Further leaching leads to the sequence spionkopite → covellite (Goble 1981).

The heat source is enigmatic. Four episodes of crustal heating on a regional scale took place after the Cambrian metamorphic event, all accompanied by igneous activity. The first magmatic event occurred during the Pampean Orogeny (Cambrian), producing metaluminous, calc-alkaline granitoid sequences; also related to a later phase of this orogeny are strongly peraluminous granitoids and pegmatites (Rapela et al. 1998). Sodium-rich trondhjemitic and granodioritic plutons were intruded during the Famatinian Orogeny (Ordovician), followed by a

pegmatite swarm (Rapela et al. 1998). The largest igneous body in the region is the Devonian Achala Batholith, dated on zircon (U–Pb) between 379 ± 4 and 368 ± 2 Ma (Dorais et al. 1997; Rapela et al. 2008). However, the nearest outcrops of the batholith are found 13 km W of the dioptase occurrence. Finally, alkaline basalts were erupted or formed dikes during an aborted Cretaceous rifting event (Kay and Ramos 1996). Fluorine remobilization leading to intragranitic fluorite mineralization, dated at 131 ± 22 Ma (La Nueva lode, inside the Achala Batholith), was possibly related to heat transfer due to this basic magmatism (Galindo et al. 1997). However, it should be stressed that there are no igneous rocks in the proximity of the dioptase occurrence.

A metamorphic origin of the fluids should be considered, given the isotopic signature of calcite and lack of related igneous bodies that otherwise could be an evident source of heat and elements. Most of the fluid-releasing reactions are likely to occur during the prograde stage (Pirajno 1992). However, the open cavities frequent in the Esperanza quarry indicate that the mineralization postdated the last metamorphic event, but any evidence for metamorphism that could have mobilized hydrothermal solutions after the marble was partially uplifted and fractured is lacking.

One alternative could be the circulation of water caused by the Tertiary uplift of Paleozoic blocks forming the Sierras Pampeanas as a result of the more westerly shortening due to the Andean Orogeny (Baldo et al. 1996a). However, this scenario remains purely speculative.

7. Conclusions

The studied marble-hosted copper mineralization at Saldán, Córdoba Province (central Argentina), consisting mainly of chrysocolla, dioptase and plancheite with very subordinate barite, is not part of the supergene zone of a metallic deposit. The copper source could not be tightly constrained by the information presented in this contribution, but the geological evidence (including isotope data) points towards copper mobilization from country rocks by very dilute hydrothermal (T ~ 300 ºC) solutions of meteoric origin. The most likely candidates are marbles (which contain small amount of Cu sulfides) or amphibolites.

Acknowledgements. SECyT-UNC provided partial financial support for this project. Beatriz Coira and Patrocinio Flores (Instituto de Geología y Minería, Jujuy) are gratefully acknowledged for the whole-rock chemical analyses. Michael Dorais (Brigham Young University, Provo) allowed RL to perform some of the electron microprobe analyses reported here. Radek Škoda (Masaryk University, Brno) kindly sent a copy of a publication on Czech dioptase. William Simmons and Alexander Falster (University of New Orleans) are thanked for access to the SEM. Jorge Sfragulla (Universidad Nacional de Córdoba) kindly brought to our attention the isotopic values of marbles from Córdoba. We are very grateful to Zdeněk Dolníček (Palacký University, Olomouc) and Martin Okrusch (Julius-Maxmilians-Universität Würzburg) for constructive and detailed reviews and to the Editors Stuart Mills, Jakub Plášil and Vojtěch Janoušek for careful editorial handling.

References

Alirezaei S, Cameron EM (2001) Variations of sulfur isotopes in metamorphic rocks from Bamble Sector, southern Norway: a laser probe study. Chem Geol 181: 23–45

Angelelli V, de Brodtkorb MK, Gordillo CE, Gay HD (1983) The Mineral Species of the Argentine Republic. Special Publication of Servicio Minero Nacional, Subsecretaría de Minería, Buenos Aires, pp 1–528 (in Spanish)

Anthony JW, Bideaux RA, Bladh KW, Nichols MC (eds) (2001) Handbook of Mineralogy. Volume I. Mineral Data Publishing, Tucson, pp 1–446

Bajnoczi B, Molnar F, Maeda K, Izawa E (2000) Shallow level, low-sulphidation type epithermal systems in the Regec Caldera, Central Tokaj Mts., NE-Hungary. Geol Carpath 51: 217–227

Baldo EG, Casquet C, Galindo C (1996a) The metamorphism of the Sierra Chica of Córdoba (Pampean Ranges), Argentina. Geogaceta 19: 51–54 (in Spanish)

Baldo EG, Demange M, Martino RD (1996b) Evolution of the Sierras de Córdoba, Argentina. Tectonophysics 267: 121–142

Bérar J-F, Lelann P (1991) E.S.D.'s and estimated probable error obtained in Rietveld refinements with local correlations. J Appl Crystallogr 24: 1–5

Brodtkorb MK de, Hillar N, Ametrano S (1981) Copper showings present in the limestone quarries of Cañada de Álvarez, Córdoba Province. In: Proceedings of the 8º Congreso Geológico Argentino, San Luis 2: pp 851–861 (in Spanish)

Brown PP (1989) FLINCOR: a microcomputer program for the reduction and investigation of fluid-inclusion data. Amer Miner 74: 1390–1393

Canfield DE (2001) Biogeochemistry of Sulfur Isotopes. In: Valley JW, Cole DR (eds) Stable Isotope Geochemistry. Mineralogical Society of America and Geochemical Society Reviews in Mineralogy and Geochemistry 43: 607–636

Cook RB (2002) Dioptase: Tsumeb, Namibia. Connoisseur's Choice. Rocks & Minerals 77: 176–180

Cook RB (2003) Letters to the Editor – dioptase update. Rocks & Minerals 78: 151–152

Cook NJ, Hoefs J (1997) Sulphur isotope characteristics of metamorphosed Cu–(Zn) volcanogenic massive sulfide deposits in the Norwegian Caledonides. Chem Geol 135: 307–324

Cook RB, Nicolson BE (2002) The occurrence of dioptase in African mineral deposits. Mineral Rec 33: 77–78

Crane MJ, Sharpe JL, Williams PA (2001) Formation of chrysocolla and secondary copper phosphates in the highly weathered supergene zones of some Australian deposits. Rec Australian Mus 53: 49–56

Craw D (1997) Fluid inclusion evidence for geothermal structure beneath the Southern Alps, New Zealand. New Zeal J Geol Geop 40: 43–52

Dalla Salda LH (1984) The intimate structure of the Sierra de Córdoba. Rev Asoc Geol Arg 39: 38–51 (in Spanish)

Daziano CO (2004) The amphibolites of the Sierra Chica of Córdoba, Argentina. Publicaciones de la Universidad Nacional de Córdoba, Córdoba, pp 1–130 (in Spanish)

Dorais MJ, Lira R, Chen Y, Tingey D (1997) Origin of biotite–apatite rich enclaves, Achala Batholith, Argentina. Contrib Mineral Petrol 130: 31–46

Fernández RR, Blesa A, Moreira P, Echeveste H, Mykietiuk K, Andrada de Palomera P, Tessone M (2008) Gold and silver deposits related to Jurassic Patagonian volcanism: review and perspectives for exploration. Rev Asoc Geol Arg 63: 665–681 (in Spanish)

Friedman I, O'Neil JR (1977) Compilation of stable isotope fractionation factors of geochemical interest. In: Fleischer M (ed) Data of Geochemistry. United States Geological Survey Professional Paper 440–KK, 6th edition, Reston, pp 1–49

Galindo C., Pankhurst RJ, Casquet C, Coniglio J, Baldo EG, Rapela CW, Saavedra J (1997) Age, Sr- and Nd-isotope systematics, and origin of two fluorite lodes, Sierras Pampeanas, Argentina. Int Geol Rev 39: 948–954

Gammons CH, Williams-Jones AE (1997) Chemical mobility of gold in the porphyry–epithermal environment. Econ Geol 92: 45–59

Gay HD, Gordillo CE, Labudía CA (1975) Plancheite $Cu_8(Si_4O_{11})_2(OH)_4 \cdot H_2O$ of the Nucha mine, Unquillo (Córdoba). Rev Asoc Arg Miner Petrol Sedim 6: 73–88 (in Spanish)

Goble RJ (1981) The leaching of copper from anilite and the production of a metastable copper sulfide structure. Canad Mineral 19: 583–591

Gordillo CE, Lencinas A (1979) Pampean Ranges of Córdoba and San Luis. In: Turner JC (ed) 2º Simposio de Geología Regional Argentina. Academia Nacional de Ciencias, Córdoba 1: 577–646 (in Spanish)

Hatert F (2005) Transformation sequences of copper sulfides at Vielsam, Stavelot Massif, Belgium. Canad Mineral 43: 623–635

Hauy R (1798) Sur la dioptase. Bul Sci Soc Phil 2: 101

Kay SM, Ramos VA (1996) The Cretaceous magmatism of the Sierra de Córdoba and its tectonic implications. In: Proceedings of the 13º Congreso Geológico Argentino, Buenos Aires, 3: 453–464 (in Spanish)

Kerrich B (1987) Stable isotope studies of fluids in the crust. In: Kyser TK (ed) Short Course in Stable Isotope Geochemistry of Low Temperature Fluids. Mineralogical Association of Canada, Saskatoon, 13: 258–286

Kim S-T, O'Neil JR (1997) Equilibrium and nonequilibrium oxygen isotope effects in synthetic carbonates. Geochim Cosmochim Acta 61: 3461–3475

Le Bail A, Duroy H, Fourquet JL (1988) Ab-initio structure determination of $LiSbWO_6$ by X-ray powder diffraction. Mater Res Bull 23: 447–452

Lira R, Ocanto C, Ripley EM (2008) Hydrogen and oxygen isotope data of epidote-group minerals: evidence for the origin of some metasomatic and deuteric-hydrothermal fluids from the Sierras Pampeanas of Córdoba, Argentina. In: Linares E, Cabaleri NG, Do Campo MD, Ducós EI, Panarello HO (eds) Proceedings of the VI South American Symposium on Isotope Geology. San Carlos de Bariloche (CD-ROM)

Luque FJ, Pasteris JD, Wopenka B, Rodas M, Barrenechea JF (1998) Natural fluid-deposited graphite: mineralogical characteristics and mechanisms of formation. Am J Sci 298: 471–498

Markham NL (1959) Occurrence of jordanite in the Otavi Mountains, South West Africa. Amer Miner 44: 682–685

Mishra B, Pal N (2008) Metamorphism, fluid flux, and fluid evolution relative to gold mineralization in the Hutti–Maski Greenstone Belt, Eastern Dharwar Craton, India. Econ Geol 103: 801–827

Moritz R (2006) Fluid salinities obtained by infrared microthermometry of opaque minerals: implications for ore deposit modeling – a note of caution. J Geochem Explor 89: 284–287

Mutti D, Di Marco A (1999) Copper–iron and lead–zinc deposits related to submarine volcanism, Córdoba. In: Zappettini EO (ed) Recursos Minerales de la República Argentina. Instituto de Geología y Recursos Minerales, SEGEMAR, Buenos Aires, Anals 35: 207–225 (in Spanish)

Mutti D, Di Marco A, Fernández S (1998) Ore deposits in the Neoproterozoic back-arc system of the central–south Sierras de Córdoba, Argentina. In: Proceedings of the 6º Congreso Nacional de Geología Económica, Buenos Aires 3: pp 81–87

Naden J, Shepherd TJ (1989) Role of methane and carbon dioxide in gold deposition. Nature 342: 7936–795

Newberg DW (1967) Geochemical implications of chrysocolla-bearing alluvial gravels. Econ Geol 62: 932–956

O'Neil JR, Clayton RN, Mayeda TK (1969) Oxygen isotope fractionation in divalent metal carbonates. J Chem Phys 51: 5547–5558

Ohmoto H, Rye RO (1979) Isotopes of sulfur and carbon. In: Barnes HL (ed) Geochemistry of Hydrothermal Deposits, 2nd edition. John Wiley and Sons, New York, pp 509–567

Olsacher J (1938) The minerals from the Córdoba Ranges. Imprenta de la Universidad Nacional de Córdoba, Córdoba, pp 1–71 (in Spanish)

Panarello HO, García CM, Valencia SA, Linares E (1980) Determination of the isotopic composition of carbon, its use in hydrogeology and geology. Rev Asoc Geol Arg 35: 460–466 (in Spanish)

Pauliš P, Škoda R, Novák F (2006) Dioptase from uranium deposit Zálesí in Rychlebské hory Mts. (Czech Republic). Čas Slez Muz Opava (A) 55: 77–79 (in Czech)

Pirajno F (1992) Hydrothermal Mineral Deposits: Principles and Fundamental Concepts for the Exploration Geologist. Springer Verlag, Berlin, pp 1–709

Poklepovic MF, Colombo F, Lira R (2001) Microthermometric data on dioptase from Esperanza quarry, Sierras Chicas, Córdoba, Argentina. Abstract. In: Noronha F, Dória A, Guedes A (eds) XVI European Current Research On Fluid Inclusions. Faculdade de Ciências do Porto, Departamento de Geologia, Memória nº 7: 373–374

Pouchou J-L, Pichoir F (1985) "PAP" (φρZ) procedure for improved quantitative microanalysis. In: Armstrong JT (ed) Microbeam Analysis. San Francisco Press, San Francisco, pp 104–106

Pudack, C, Halter, WE, Heinrich, CA, Pettke, T (2009) Evolution of magmatic vapor to gold-rich epithermal liquid: the porphyry to epithermal transition at Nevados de Famatina, northwest Argentina. Econ Geol 104: 449–477

Rapela CW, Pankhurst RJ, Casquet C, Baldo E, Saavedra J, Galindo C, Fanning CM (1998) The Pampean Orogeny of the southern proto-Andes: Cambrian continental collision in the Sierras de Córdoba. In: Pankhurst RJ, Rapela CW (eds) The Proto-Andean Margin of Gondwana. Geological Society London Special Publications 142: 181–217

Rapela CW, Baldo EG, Pankhurst R, Fanning CM (2008) The Devonian Achala Batholith of the Sierras Pampeanas: F-rich, aluminous A-type granites. In: Linares E, Cabaleri NG, Do Campo MD, Ducós EI, Panarello HO (eds) Proceedings of the VI South American Symposium on Isotope Geology. San Carlos de Bariloche (CD-ROM)

Richards JP, Spooner ETC (1989) Evidence for Cu–(Ag) mineralization by magmatic–meteoric fluid mixing in Keweenawan fissure veins, Mamainse Point, Ontario. Econ Geol 84: 360–385

Roisnel T, Rodríguez-Carvajal J (2001) WinPLOTR: a Windows tool for powder diffraction pattern analysis. In: Delhez R, Mittemeijer EJ (eds) Materials Science Forum, Proceedings of the Seventh European Powder Diffraction Conference (EPDIC 7, Barcelona), 118–123

Rosenbaum J, Sheppard SMF (1986) An isotopic study of siderites, dolomites, and ankerites at high temperatures. Geochim Cosmochim Acta 50: 1147–1150

Rusk BG, Reed MH (2008) Fluid inclusion evidence for magmatic–hydrothermal fluid evolution in the porphyry copper–molybdenum deposit at Butte, Montana. Econ Geol 103: 307–334

Russell B, Jens G, Harald S, Eva S, Craig M (2010) Sulfur isotope characteristics of metamorphosed Zn–Cu volcanogenic massive sulfides in the Areachap Group, Northern Cape Province, South Africa. Miner Depos 45: 481–496

Rye RO, Ohmoto H (1974) Sulfur and carbon isotopes and ore genesis: a review. Econ Geol 69: 826–842

Sato M (1960) Oxidation of sulfide ore bodies. 1. Geochemical environments in terms of Eh and pH. Econ Geol 55: 928–961

Seal II RR (2006) Sulfur Isotope Geochemistry of Sulfide Minerals. In: Vaughan DJ (ed) Sulfide Mineralogy and Geochemistry. Mineralogical Society of America and Geochemical Society Reviews in Mineralogy and Geochemistry 61: 633–677

Seal II RR, Rye RO (1993) Stable isotope study of fluid inclusions in fluorite from Idaho: implications for continental climates during the Eocene. Geology 21: 219–222

Sfragulla J, Jerez D, Bonalumi A (1999) Marbles and other carbonate rocks from Córdoba. In: Zappettini EO (ed) Recursos Minerales de la República Argentina. Instituto de Geología y Recursos Minerales SEGEMAR, Buenos Aires, Anals 35: 271–295 (in Spanish)

Sillitoe RH (2010) Porphyry copper systems. Econ Geol 105: 3–41

Turchyn AV, Schrag DP, Coccioni R, Montanari A (2009) Stable isotope analysis of the Cretaceous sulfur cycle. Earth Planet Sci Lett 285: 115–123

Vochten R, Janssens J, Blaton N (2005) Reinvestigation of dioptase–planchéite pseudomorphs after calcite from the Tantara copper deposit, Katanga, Republique du Congo. Miner Rec 36: 521–524

Walstrom RE (2006) Chasing the green goddess: dioptase in New Mexico. New Mex Geol 28: 110

Whitney DL, Evans BW (2010) Abbreviations for names of rock-forming minerals. Amer Miner 95: 185–187

Williams SA (1962) Paramelaconite and associated minerals from the Algomah Mine, Ontonagon County, Michigan. Amer Miner 47: 778–779

Witt WK, Knight JT, Mikucki EJ (1997) A synmetamorphic lateral fluid flow model for gold mineralization in the Archean southern Kalgoorlie and Norseman terranes, Western Australia. Econ Geol 92: 407–437

Yates DM, Joyce KJ, Heaney PJ (1998) Complexation of copper with polymeric silica in aqueous solution. Appl Geochem 13: 235–241

Zhang X, Nesbitt BE, Muehlenbachs K (1989) Gold mineralization in the Okanagan Valley, southern British

Columbia: fluid inclusion and stable isotope studies. Econ Geol 84: 410–424

Zheng YF (1999) Oxygen isotope fractionation in carbonate and sulphate minerals. Geochem J 33: 109–126